Bulletin of the Seismological Society of America, Vol. 102, No. 3, pp. 909–917, June 2012, doi: 10.1785/0120110008

Including Foreshocks and Aftershocks in Time-Independent Probabilistic Seismic-Hazard Analyses

by Oliver S. Boyd

Abstract Time-independent probabilistic seismic-hazard analysis treats each source as being temporally and spatially independent; hence foreshocks and aftershocks, which are both spatially and temporally dependent on the mainshock, are removed from earthquake catalogs. Yet, intuitively, these earthquakes should be considered part of the seismic hazard, capable of producing damaging ground motions. In this study, I consider the mainshock and its dependents as a time-independent cluster, each cluster being temporally and spatially independent from any other. The cluster has a recurrence time of the mainshock; and, by considering the earthquakes in the cluster as a union of events, dependent events have an opportunity to contribute to seismic ground motions and hazard. Based on the methods of the U.S. Geological Survey for a high-hazard site, the inclusion of dependent events causes ground motions that are exceeded at probability levels of engineering interest to increase by about 10% but could be as high as 20% if variations in aftershock productivity can be accounted for reliably.

Introduction

The U.S. Geological Survey produces time-independent probabilistic seismic-hazard maps, primarily for engineering purposes (Frankel *et al.*, 1996). Because these maps are time independent, reflecting Poissonian distributed seismicity (i.e., earthquake sources are independent of each other in space and time), foreshocks and aftershocks are removed from earthquake catalogs and not considered in the probabilistic seismic-hazard analysis (PSHA). However, intuitively, these temporally and spatially dependent events should contribute to seismic hazard and be considered in the time-independent analysis.

Aftershocks have been incorporated into what is considered aftershock probabilistic seismic-hazard analysis (APSHA; see Wiemer [2000] and Yeo and Cornell [2009]), which is the hazard due to aftershocks after the occurrence of a mainshock. APSHA is particularly useful in the hours to days after a major earthquake to help guide response and recovery efforts. It differs from the method presented in this paper in that APSHA is predicated on a known mainshock, is applicable to relatively short time horizons, and is a time-dependent analysis (hazard changes with time). The method proposed in this paper is time-independent and is intended to be applicable for the lifetime of engineered structures.

To incorporate foreshocks and aftershocks into time-independent PSHA, I consider that for a given mainshock, the mainshock and its associated foreshocks and aftershocks each have an opportunity to exceed a given amount of ground motion at a site. This cluster of earthquakes is then considered to be a time-independent event, each cluster being spatially and temporally unrelated to any other cluster.

A Union of Events

The concept of incorporating earthquake clustering in probabilistic seismic-hazard analysis was first proposed by Toro and Silva (2001) for the 1811–1812 series of earthquakes in the New Madrid Seismic Zone, denoted in Figure 1 as events 1–3. These earthquakes, having magnitudes >7 (Johnston, 1996a; Hough *et al.*, 2000; Bakun and Hopper, 2004) and a recurrence interval of about 500 years (Tuttle *et al.*, 2002), occurred within a two-month period (Johnston, 1996b). Paleoseismic evidence suggests that this clustering of large events is a recurring phenomenon (Tuttle *et al.*, 2002; 2005). In previous time-independent probabilistic seismic-hazard analyses (Frankel *et al.*, 2002), for a given site (e.g., Memphis), the closest of the three events was used while ignoring the other two, considering them something akin to aftershocks. Toro and Silva (2001) argued that each event should be able to contribute to seismic hazard and proposed that these three events should form a mathematical union for which, at a particular site, each event in the cluster has an independent probability of exceeding a specified ground motion; either event 1 or event 2 or event 3 can exceed ground-motion z. If I consider these probabilities, p_1, p_2, and p_3, as representing areas, this would be analogous to a Venn diagram (Venn, 1880) in which the total area spanned by the overlapping probabilities p_1, p_2, and p_3 is the probability p_c

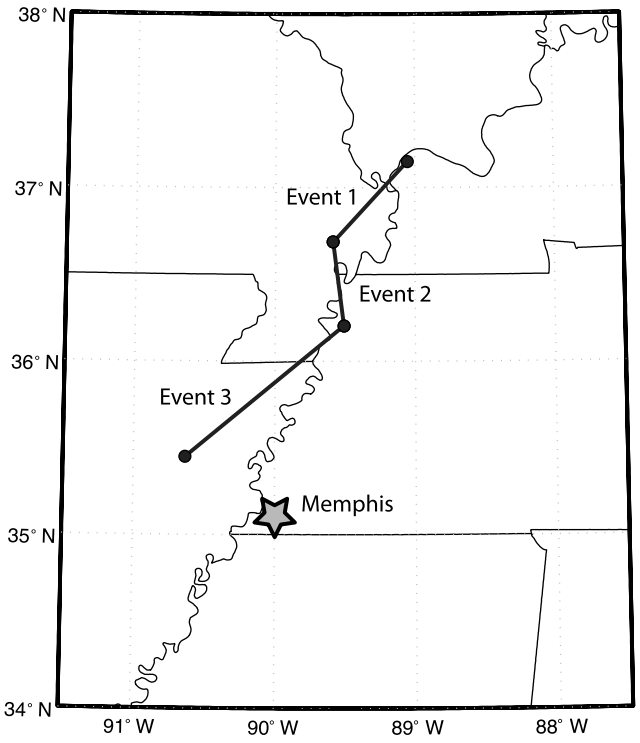

Figure 1. Southern, central, and northern fault strands of the New Madrid Seismic Zone used in the 2008 update of the U.S. National Seismic Hazard maps. These strands were combined in a clustered analysis as outlined in this paper.

that the cluster will exceed ground-motion z (Fig. 2) and is equal to

$$p_c = p_1 + p_2 + p_3 - (p_1p_2 + p_1p_3 + p_2p_3) + p_1p_2p_3. \quad (1)$$

The cluster exceedance probability is equal to the sum of the individual earthquake exceedance probabilities minus the intersection of each pair plus the intersection of all three.

This expression can be reorganized such that the cluster exceedance probability is interpreted to reflect the probability that no event in the cluster is unable to exceed a specified ground motion or, conversely, that at least one event in the cluster is able to exceed a specified ground motion. In this form, p_c can be written

$$p_c = 1 - (1 - p_1)(1 - p_2)(1 - p_3). \quad (2)$$

It is now straightforward to generalize this expression for any number of events. Equation (2) becomes

$$p_c = 1 - \prod_{i=1}^{n}(1 - p_i). \quad (3)$$

As any of the individual exceedance probabilities, p_i, approach 1, the term on the right approaches 0, and the cluster exceedance probability approaches 1. Conversely, as the

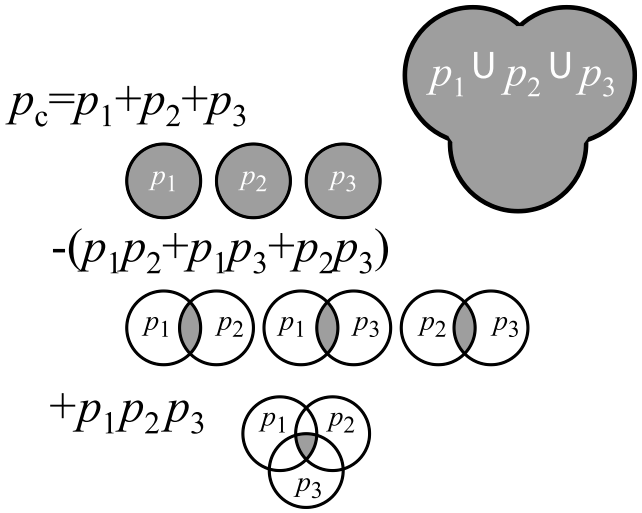

Figure 2. Venn diagram illustrating the combination of individual ground-motion exceedance probabilities.

individual exceedance probabilities approach 0, all of the cross products (e.g., those that appear in equation 1) become exceedingly small relative to the individual probabilities, and the cluster exceedance probability tends to a sum of the individual exceedance probabilities. It is important to remember that even though the foreshocks and aftershocks are spatially and temporally dependent on the mainshock, I assume that the probability of any event exceeding a specified ground motion is independent of the other events in the cluster.

Figure 3 is a simple illustration of these limits for the case of three events, each having an independent probability of exceeding a specified ground motion. As any of the individual exceedance probabilities approach one, the ratio of the cluster exceedance probability to the individual exceedance

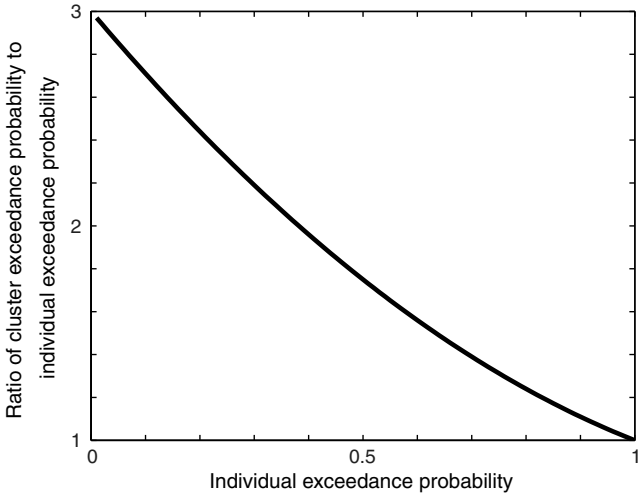

Figure 3. The relation between individual and cluster ground-motion exceedance probabilities for a case of three events of equal probability.

probability approaches one. The earthquake with the greatest probability of exceeding a given ground motion dominates. However, as the individual exceedance probabilities decrease, which is the case for larger ground motions, the ratio of the cluster exceedance probability to the individual exceedance probability approaches the number of events—in this case, a value of three. The probability of exceeding a given ground motion becomes additive. Each earthquake can then contribute independently to seismic hazard.

The New Madrid Cluster of Earthquakes

To be more specific, Figure 4 presents hazard curves for a location equidistant from the three segments of the New Madrid Seismic Zone. In this example, the ground-motion attenuation relationship of Toro *et al.* (1997) is assumed. Overlain on this figure are the probability levels of engineering interest—the ground motions that are exceeded with a 2%, 5%, and 10% chance in 50 years. For example, in accordance with the black curve in Figure 4, which represents hazard from one of the three fault segments, there is a 2% chance in 50 years of exceeding 0.3g. For very low ground motions, the probability of exceedance is close to one, and the annual rate of exceeding these low ground motions is equal to the recurrence rate of the earthquake, or once every 500 years. As the ground motions increase, they become less probable, and the rate of exceeding them decreases.

If I consider all three New Madrid earthquakes as independent events, then I produce the red curve in Figure 4. The rate of exceeding all ground-motion levels increases by 200%, or a factor of 3. The increase in the ground motions that have a 2% and 5% chance in 50 years of being exceeded is 44% and 73%, respectively.

However, because these three events tend to occur together, they cannot be treated independently but rather as a cluster. The blue curve results from equation (1). At ground motions far less than the median, which have a high probability of occurrence, the individual probabilities are close to 1, such that the clustered hazard curve approaches that of an individual event. Nevertheless, as the ground motions increase and their respective probabilities decrease, they become additive and the clustered hazard curve approaches the curve in which the events were treated independently. The ground motions at 2% and 5% in 50 years is greater than that of an individual event by 41% and 58%, respectively, but is reduced relative to treating all events independently.

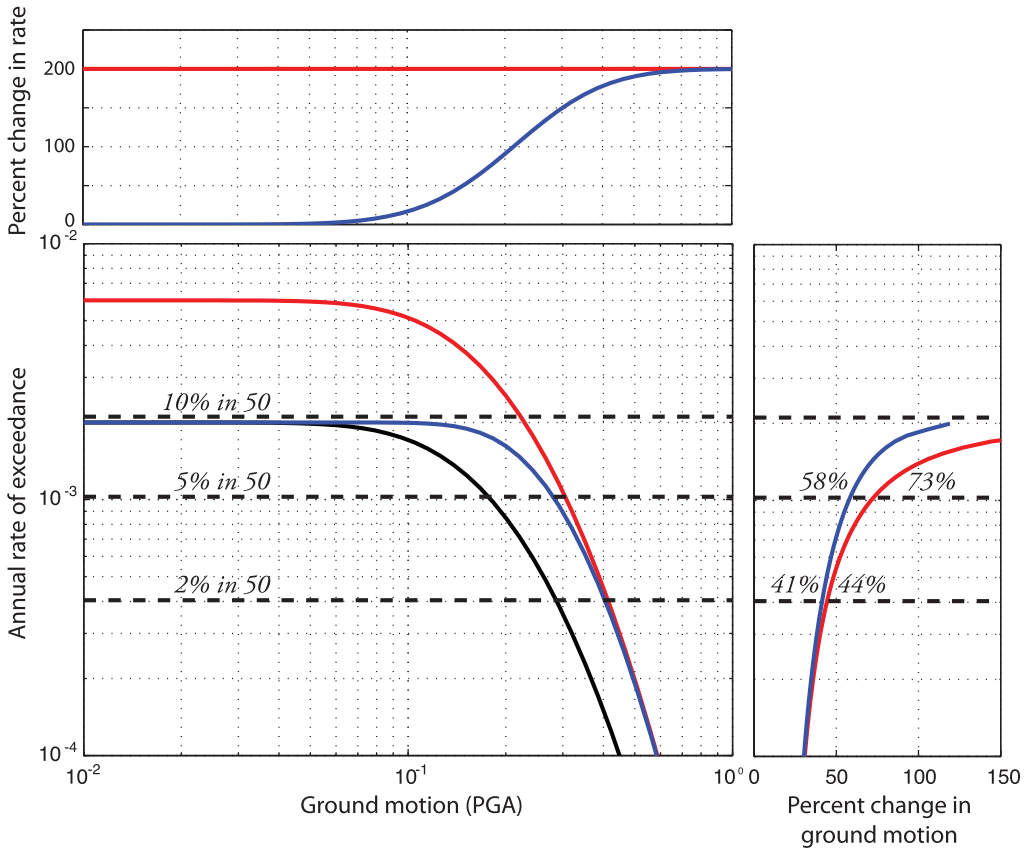

Figure 4. The effect of clustering on a hazard curve (central box) for a site located equidistant from the faults depicted in Figure 1. The black curve is a single event; the red curve, all three events; and the blue curve, a clustered analysis. The upper box shows the increase in the rate of exceeding a given amount of peak ground acceleration. The box to the right shows the increase in the peak ground acceleration that is exceeded with a given probability.

Including Foreshocks and Aftershocks

I now turn my attention to applying this clustering algorithm to foreshocks and aftershocks in the San Francisco Bay area and examine its effect on gridded seismicity-based hazard curves for San Jose, California. This hazard analysis does not contain all earthquake sources and should not be considered a complete estimate of seismic hazard in San Jose. I would attempt this analysis in the New Madrid region but am not confident that I can adequately decluster the earthquake catalog using standard declustering algorithms.

In Figure 5a, I show a full earthquake catalog for events greater than M 4 for the San Jose area. Temporally and spatially dependent events (foreshocks and aftershocks) are removed using the Gardner and Knopoff (1974) declustering algorithm in order to assess the impact of including dependent events in the U.S. National Seismic Hazard Maps (Frankel *et al.*, 2002; Petersen *et al.*, 2008). The resulting

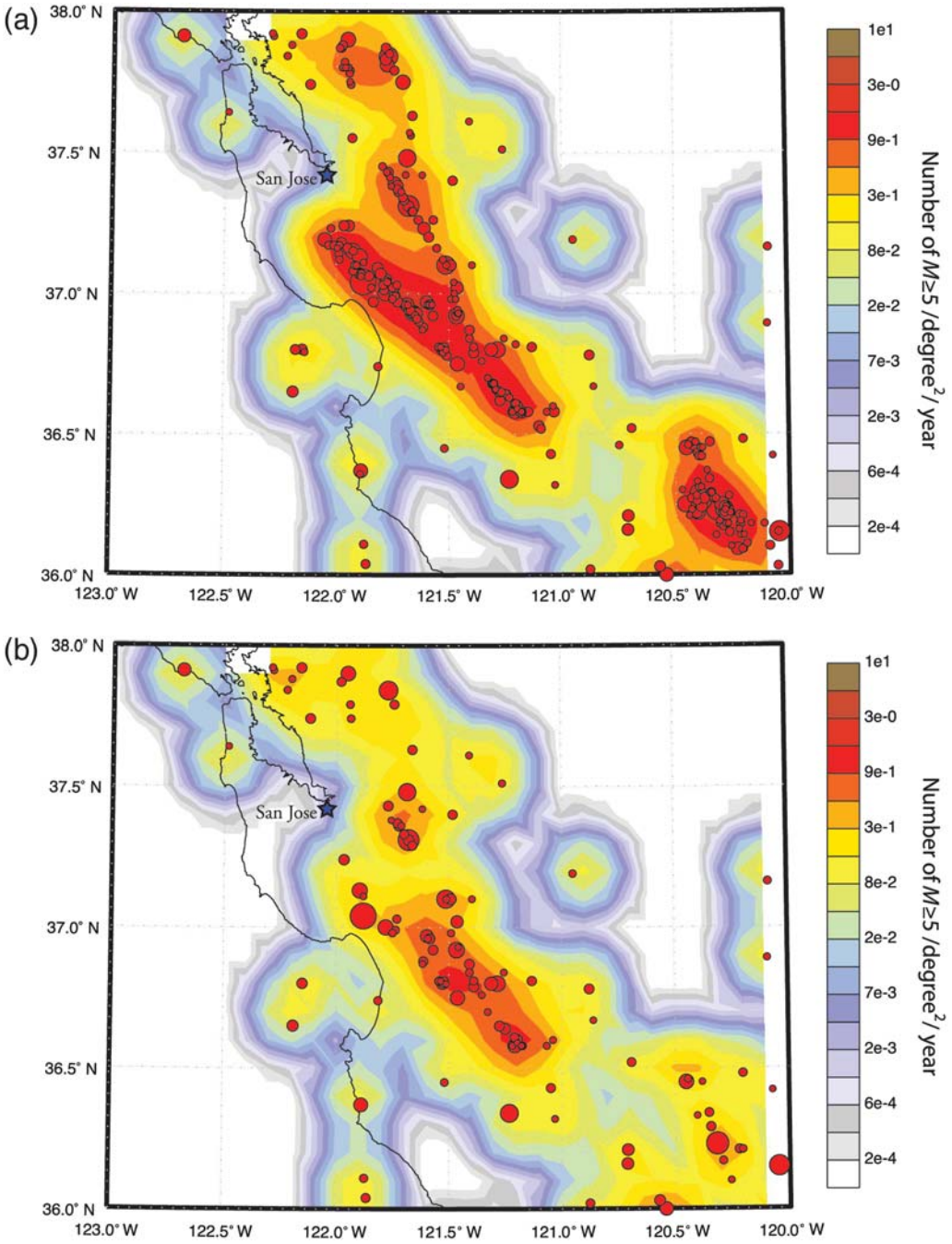

Figure 5. (a) Full and (b) declustered earthquake catalogs near San Jose, California. The color shading reflects variations in a-value and is the number of $M \geq 5$ earthquakes occurring per degree^2 per year.

catalog is shown in Figure 5b. Nearly 50% of the events have been removed from the original catalog.

To facilitate the use of these catalogs in PSHA, I assume a Gutenberg–Richter relationship and a spatially invariant b-value and calculate smoothed a-value grids constrained by the total seismic moment within each $0.1° \times 0.1°$ cell. The original and declustered catalogs have b-values of 0.95 and 0.85, respectively. The shaded maps in Figures 5a and 5b result from these b-values and smoothed a-value grids and represent the number of $M \geq 5$ earthquakes that occur per degree^2 per year. Declustering generally decreases the rate of earthquakes, but the decrease is not spatially uniform.

I produce hazard curves for San Jose using gridded earthquake sources in which I sum the rates of exceeding a given ground motion due to mainshock sources exponentially distributed between magnitudes 5 and 7.9 for all grid cells within 200 km of San Jose. This differs from the U.S. national maps for this location in the following ways: The U.S. national maps implement a complex combination of gridded, fault, and geodetically derived source models. For locations more than 10 km away from fault sources, the maximum magnitude for the gridded seismicity model is 7. Within 10 km, the maximum magnitude for the gridded source model is 6.5 when the fault source is exponentially distributed between M 6.5 and the fault's maximum magnitude and the lesser of 7 or the fault source magnitude when the fault source is characteristic. For simplicity and illustration, I assess the impact of including foreshocks and aftershocks using only strike-slip gridded sources even though the method can be applied in precisely the same way to the other sources in the U.S. national maps.

When including foreshocks and aftershocks, a synthetic set of earthquakes for each mainshock source is produced (described in the next section, Synthesizing an Earthquake Catalog), and the probability that the cluster p_c, which includes foreshocks, mainshock, and aftershocks, will exceed a given ground motion is found using equation (3). Again, the probability p_i that any individual earthquake exceeds a given ground motion is found using ground-motion attenuation relations. Whereas in the analysis for the New Madrid cluster of earthquakes I consider a single ground-motion attenuation relation, I consider the three ground-motion relations that are part of the Next Generation Attenuation project (Power *et al.*, 2008), which are used in the 2008 update of the U.S. National Seismic Hazard Maps (Petersen *et al.*, 2008), in the hazard curves for San Jose. Of the three ground-motion attenuation relations implemented (Boore and Atkinson, 2008; Campbell and Bozorgnia, 2008; Chiou and Youngs, 2008), that of Chiou and Youngs contains a term for aftershocks. This term causes the median ground motions for aftershocks in their relations to decrease by 25% and 18% and ground-motion variability to increase by about 10%–15% and 2% for peak ground acceleration (PGA) and 1-Hz spectral acceleration (SA), respectively. As is done in the U.S. National Seismic Hazard Maps, I truncate the ground motions for a given event at three times the standard deviation.

The probability that the cluster exceeds a given ground motion is then multiplied by the annual rate of the cluster r_c, which is equal to the annual rate of mainshock occurrence, to find the annual rate r of exceeding a given ground motion. The hazard curve accounting for foreshocks, mainshock, and aftershocks can be expressed as

$$r = \sum r_c p_c. \tag{4}$$

Synthesizing an Earthquake Catalog

To incorporate foreshocks and aftershocks into PSHA, I use the a-value grid resulting from the declustered catalog and create multiple synthetic sets of foreshocks and aftershocks with which to do the clustering analysis. Alternatively, I could simply use the events identified as foreshocks and aftershocks from the Gardner–Knopoff analysis. However, this would be one of many realizations, and there is no guarantee that the next set of foreshocks and aftershocks would have the same magnitudes and spatial distribution.

For each mainshock and each of 20 iterations of the PSHA analysis, I generate a set of related foreshocks and aftershocks according to a modified Gutenberg–Richter relation for aftershocks as presented by Shcherbakov *et al.* (2004),

$$N(\geq M) = 10^{b'(m_{ms}-\Delta m-m)}, \tag{5}$$

where N is the number of aftershocks greater than or equal to magnitude m, b' is the b-value for the aftershock catalog, m_{ms} is the mainshock magnitude, and Δm is the magnitude difference between the largest aftershock and the mainshock. I choose b' and Δm that result in a full catalog (declustered plus synthetic) that matches the Gutenberg–Richter statistics of the original catalog. Because all of the synthesized foreshocks and aftershocks are part of the cluster for a given mainshock, it does not matter when the events occur. Hence, the use of an Omori law is not needed.

I perform a grid search with a range of b' and Δm from 0.6 to 1.2 and 0.75 to 1.4, respectively, attempting to minimize a misfit function. The misfit function is defined as the absolute difference between the log of the incremental number of occurrences of earthquakes in the original catalog and the log of the incremental number of occurrences of earthquakes in the full synthetic catalog for magnitudes between 5 and 7.9 with an increment of 0.1. The value of b' and Δm that best fit the original catalog are both close to 1, as shown by the red star in Figure 6. For the remainder of the analysis, I choose a b' of 0.96 and a Δm of 1.05, though any particular catalog and choice of declustering algorithm will result in a slightly different value of b' and Δm.

One parameter that has some significance is the placement of foreshocks and aftershocks. Felzer and Brodsky (2006) found that the decay of the density of aftershocks with distance from the mainshock follows an inverse power law.

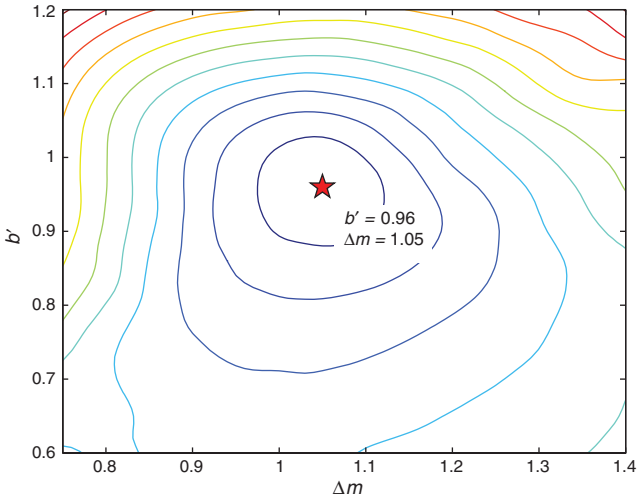

Figure 6. Contours of the misfit function in the determination of Δm and b'. The misfit function is defined as the sum of the absolute difference between the log of the incremental number of earthquakes in the original catalog minus the log of the incremental number of earthquakes in the full synthesized catalog for magnitudes between 5.0 and 7.9 with an increment of 0.1. The red star represents the minimum misfit and corresponds to a Δm of 1.05 and b' of 0.96.

Yeo and Cornell (2009), on the other hand, assumed that in their study aftershocks were either uniformly distributed along the fault rupture or concentrated at the ends.

With the aftershocks identified by the Gardner–Knopoff (G-K) declustering algorithm, I examine the decay of aftershock density with distance and whether I can confidently identify and place aftershocks along a linear trend. Like Felzer and Brodsky, I find an inverse power law decay of aftershock density with distance from the mainshock (Fig. 7a). The power law exponent I find is closer to −1.0, whereas they find −1.35. They however consider aftershocks within 5 minutes and 50 km of mainshock magnitudes down to M 2, while I use the aftershocks within the G-K time and distance windows for mainshock magnitudes greater than M 4 (the time and distance window for an M 4 earthquake is 42 days and 30 km).

Aftershocks within the G-K windows rarely line up along a single linear trend. When I attempt to locate the fault with aftershocks by considering the orientation that maximizes the ratio of the standard deviation of fault parallel aftershock locations to the standard deviation of fault perpendicular aftershock locations for each aftershock cluster, I generally find significant off-fault activity. Figure 7b shows the percentage of aftershock clusters with a given ellipticity and indicates that aftershocks are more likely to have a relatively uniform azimuthal distribution about the mainshock. Other declustering algorithms may lead to alternate spatial dependence, but, again, an analysis with G-K is used here in order to help assess the impact of including dependent events in the U.S. national maps. A more comprehensive study of the spatial dependence of foreshocks and aftershocks is beyond the scope of this paper.

I therefore distribute aftershocks in the synthetic catalog such that the density decays with distance according to an inverse power law with an exponent of −1.0. I assume a uniform azimuthal distribution but consider, in the discussion, that dependent events could be distributed along a single azimuth parallel to the San Andreas fault.

In summary, the hazard is a product of the occurrence rate of the cluster times the probability that the cluster will exceed a given ground motion. The probability that the cluster exceeds a given ground motion is given by equation (3), in which each individual exceedance probability, calculated using ground-motion attenuation relations, corresponds to the mainshock and each of its dependent events.

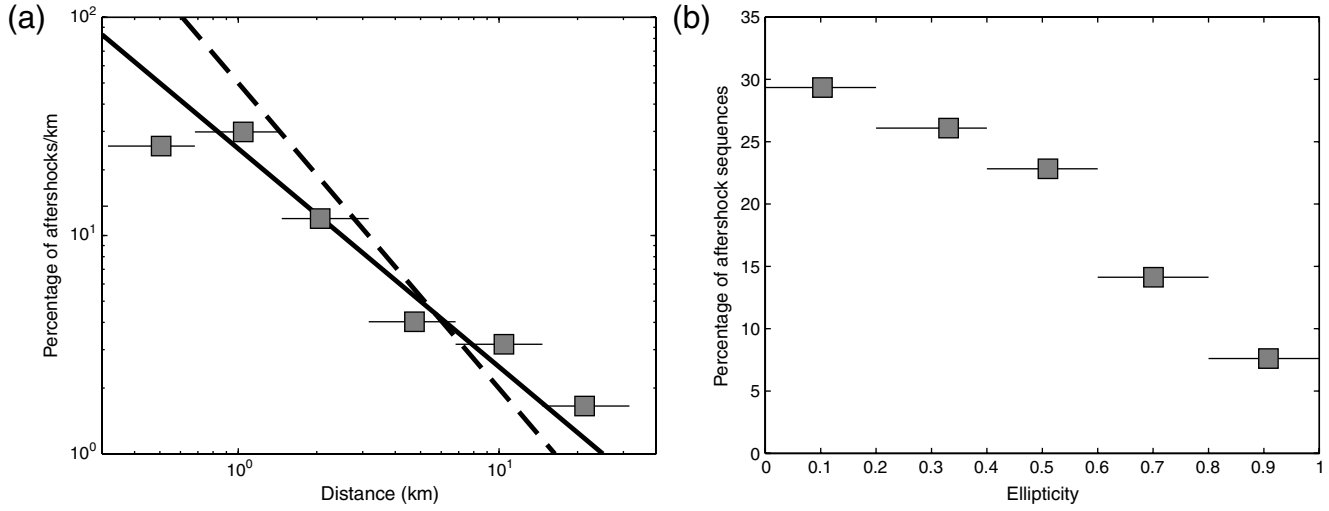

Figure 7. Distribution of aftershocks about mainshock. (a) The density of aftershocks with distance from the mainshock decays approximately as r^{-1} (solid line; dashed line is $r^{-1.4}$). (b) Aftershocks are more likely to have a relatively uniform azimuthal distribution (small ellipticity) than to lie along a linear trend (ellipticity of 1). The symbols in (a) and (b) are averages of the data within the bins defined by the horizontal lines.

Clustered Hazard Curves for San Jose

The black curves in Figures 8b and 8e reflect PGA and 1-Hz SA hazard curves for San Jose using only the declustered catalog. I have established that a hazard curve properly accounting for foreshocks and aftershocks should not exceed an analysis using a full catalog where foreshocks, mainshocks, and aftershocks are treated independently. Hazard calculated using the original catalog is one such realization (green curves in Figure 8) and leads to increased rates of exceeding ground motions greater than 0.1*g* PGA or 1-Hz SA by 70%–120%. The ground motions that are exceeded at probability levels of engineering interest, that is, 2%, 5%, and 10% probability of exceedance in 50 years, increase by 20%–30%. For an analysis of full synthesized catalogs in which all events are treated independently and uniformly distributed azimuthally about the mainshock (red curves in Fig. 8), annual rates of exceeding ground motions greater than 0.1*g* PGA and 1-Hz SA increase by about 50%. Ground motions at probability levels of engineering interest increase between 12% and 17% for PGA and between 14% and 19% for 1-Hz SA. When the mainshock and its associated foreshocks and aftershocks are considered as a cluster (blue curves in Fig. 8), the annual rates of exceeding ground motions greater than 0.1*g* PGA and 1-Hz SA increase from 15% to 30% and ground motions at probability levels of engineering interest increase by about 10%.

Discussion

At a site located in San Jose, California, the clustered analysis begins to approach an analysis in which foreshocks and aftershocks are treated as independent events for probability levels less than a 10% chance of exceedance in 50 years. The difference between the two types of analyses depends on the *a*-value or rate of earthquakes. As the rate of earthquakes near a site decreases, the rate of exceeding a particular ground motion decreases. In other words, the hazard curves move down the *y* axis. This causes the transition at which the two analyses become relatively similar to occur at lower probability levels. Hence in regions far from relatively active faults where seismicity is low, seismic hazard at probability levels of engineering interest may be more like an analysis done on a declustered catalog, whereas close to relatively active faults where seismicity is high, it may be more like an analysis in which all events in the original catalog are treated independently.

A comparison between an analysis performed with the original nondeclustered catalog containing foreshocks and aftershocks (green curves in Fig. 8) and an analysis using the

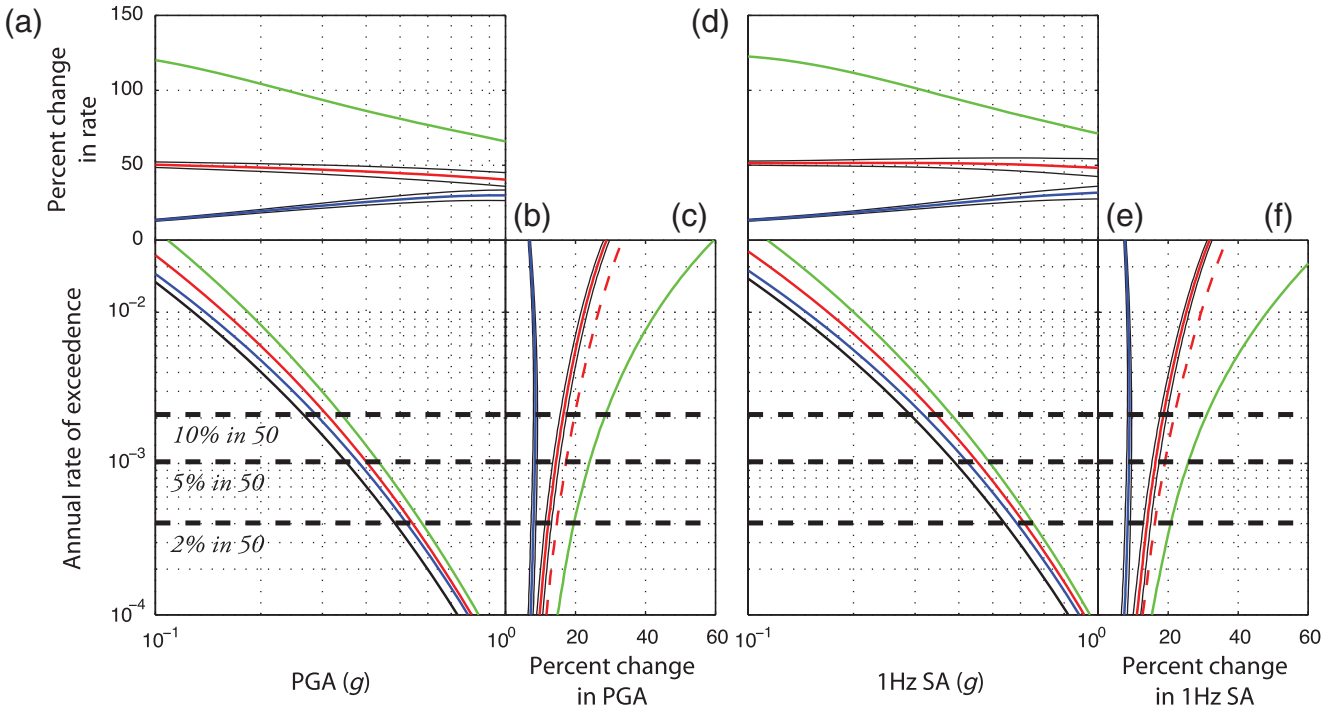

Figure 8. Hazard curves (b, e) and changes in annual rates (a, d) and ground motions (c, f) at probabilities of engineering interest for San Jose, California: (a–c) are for PGA, (d–f) are for 1-Hz SA. In (b) and (e): black curves, traditional analysis with a declustered catalog; green curves, a traditional analysis using the original nondeclustered catalog; red curves, a full catalog where foreshocks and aftershocks are synthesized and have either a uniform azimuthal distribution (solid curves) or are distributed along an azimuth of N45°W (dashed curves) and all events are treated independently; and blue curves, an analysis where the mainshocks and associated foreshocks and aftershocks are treated as a cluster and have a uniform azimuthal distribution.

declustered catalog with synthetic sets of foreshocks and aftershocks (red curves in Fig. 8), where in both analyses all earthquakes are treated independently, reveals several inadequacies in this estimation of seismic hazard and seismic-hazard estimation in general. Even though I consider multiple realizations of the synthetic catalog, the analysis performed with the original catalog lies well outside one standard deviation of an analysis with full synthesized catalogs. There are two factors that likely contribute significantly to this effect.

First, in the analysis presented in this paper, catalogs of foreshocks and aftershocks were synthesized according to a modified Gutenberg–Richter law such that the Gutenberg–Richter statistics of the declustered plus synthetic catalogs matched that of the original catalog containing foreshocks and aftershocks. I determine and use a single value of b' and Δm. It is likely that these values vary spatially (Wiemer and Katsumata, 1999) and temporally and contribute to locally high rates of seismicity near San Jose. In this case, the values of b' and Δm that are required to match the two hazard analyses for San Jose are 1.1 and 0.7, respectively.

A second factor contributing to the difference between the two hazard analyses is related to how the foreshocks and aftershocks are distributed about the mainshock. I distribute them with a uniform azimuthal distribution about the mainshock and a distance from the mainshock that decays according to an inverse power law. It is possible however that foreshocks and aftershocks will lie along a linear trend and occur on average closer to San Jose, though, as is shown in Figure 7, the foreshocks and aftershocks identified using the Gardner–Knopoff method rarely lie along a single linear trend. To investigate the effect of a limited azimuthal distribution of foreshocks and aftershocks, an analysis is performed in which foreshocks and aftershocks are placed along an orientation roughly parallel to the San Andreas fault, N45°W. This causes the hazard at probability levels of engineering interest to increase by about 2%–3% (dashed red curves in Fig. 8), far less than that needed to match an analysis performed with the original catalog. The spatial distribution of aftershocks therefore can explain only a small part of the discrepancy.

The more general problem of declustering earthquake catalogs is a critical issue in this analysis and seismic-hazard analyses in general. The Gardner–Knopoff method was used here in order to illustrate the effect of adding foreshocks and aftershocks to the U.S. national maps. Other declustering methods may or may not be more appropriate for seismic-hazard analyses, but investigating this problem is beyond the scope of this study.

The Gardner–Knopoff method removes all earthquakes within a certain time and distance window of the mainshock. The size of the windows is a function of magnitude and was derived for California earthquakes. Not only is it not strictly correct to remove every earthquake in these windows, these windows may be far different outside of California. Further, the size of these windows may vary spatially and temporally. All of these issues should be considered in estimating the full uncertainty of seismic-hazard estimates. Other methods of declustering earthquake catalogs include, for example, that of Reasenberg (1985) in which pairs of earthquakes close in space and time are associated to form clusters and removed from earthquake catalogs or those based on epidemic-type aftershock sequences (Zhuang *et al.*, 2002; Hainzl *et al.*, 2006) in which events are removed with some probability of being part of a cluster. It is possible that these methods would have declustered the original earthquake catalog in such a way that a strong spatial variation in aftershock productivity would not have been inferred, thereby reducing the difference between the analysis on the original undeclustered catalog and the declustered catalog with synthesized foreshocks and aftershocks. Additional work should focus on a comparison of declustering algorithms and the variability of the parameters that define them.

Conclusions

Foreshocks and aftershocks are incorporated into time-independent probabilistic seismic-hazard analyses by mathematically considering the cluster of foreshocks, mainshock, and aftershocks as a union of events in which each event in the cluster has some probability of exceeding a given ground motion. The cluster, then, is considered time independent. The proposed method is used on a western U.S. earthquake catalog that is declustered with the Gardner–Knopoff declustering algorithm in order to assess the effect of including dependent events in the U.S. National Seismic Hazard maps. Multiple realizations of foreshocks and aftershocks are reintroduced to the catalog assuming a modified Gutenberg–Richter relation, and hazard curves are calculated. Although this method was employed on what is considered a gridded seismicity source model, it can also be used in precisely the same way for fault and geodetically derived source models.

For a high hazard site in California, PGA and 1-Hz SA hazard estimates increase by about 10%. Increases in hazard based on the original undeclustered catalog are twice that of synthetic catalogs in which each event in the synthetic catalog is treated independently. This result indicates that the Gardner–Knopoff declustering algorithm removed too many earthquakes near the site of the hazard analysis (and too few elsewhere) and/or the presence of a strong spatial variation in the productivity of aftershocks.

In general, I find that at relatively high rates of seismic activity, such as in many parts of the western United States, and at probability levels of engineering interest, the clustered analysis will approach an analysis in which foreshocks, mainshocks, and aftershocks are treated as independent events.

Data and Resources

All data referred to in this paper come from published sources, which are listed in the references section. Plots were made using MathWorks MATLAB, v. R2010B (www

.mathworks.com, last accessed September 2010). Additional annotation in the figures was accomplished with Adobe Illustrator CS4 (www.adobe.com/Illustrator, last accessed September 2009).

Acknowledgments

Members of the National Seismic Hazard Mapping Project including Mark Petersen, Chuck Mueller, and Nico Luco provided invaluable insight into probabilistic seismic-hazard analysis, declustering of earthquake catalogs, and earthquake clustering. Morgan Page and Dave Perkins provided thorough reviews, which helped to clarify and elucidate important distinctions. Additional reviews by three anonymous reviewers and Peter Stafford further improved the manuscript.

References

Bakun, W. H., and M. G. Hopper (2004). Magnitudes and locations of the 1811–1812 New Madrid, Missouri, and the 1886 Charleston, South Carolina, earthquakes, *Bull. Seismol. Soc. Am.* **94,** no. 1, 64–75.

Boore, D. M., and G. M. Atkinson (2008). Ground-motion prediction equations for the average horizontal component of PGA, PGV, and 5%-damped PSA at spectral periods between 0.01 s and 10.0 s, *Earthq. Spectra* **24,** no. 1, 99–138.

Campbell, K. W., and Y. Bozorgnia (2008). Ground motion model for the geometric mean horizontal component of PGA, PGV, PGD and 5% damped linear elastic response spectra for periods ranging from 0.01 to 10.0 s, *Earthq. Spectra* **24,** no. 1, 139–172.

Chiou, B. J., and R. R. Youngs (2008). An NGA model for the average horizontal component of peak ground motion and response spectra, *Earthq. Spectra* **24,** no. 1, 173–216.

Felzer, K. R., and E. E. Brodsky (2006). Decay of aftershock density with distance indicates triggering by dynamic stress, *Nature* **441,** 735–738.

Frankel, A., M. D. Petersen, C. S. Mueller, K. M. Haller, R. L. Wheeler, E. V. Leyendecker, R. L. Wesson, S. C. Harmsen, C. H. Cramer, D. M. Perkins, and K. S. Rukstales (2002). Documentation for the 2002 update of the National Seismic-Hazard Maps, *U.S. Geol. Surv. Open-File Rept. 02-420*, 33 pp.

Frankel, A., C. Mueller, T. Barnhard, D. Perkins, E. Leyendecker, N. Dickman, S. Hanson, and M. Hopper (1996). National Seismic-Hazard Maps—Documentation June 1996, *U.S. Geol. Surv. Open-File Rept. 96-532*, 110 pp.

Gardner, J. K., and L. Knopoff (1974). Is the sequence of earthquakes in southern California, with aftershocks removed, Poissonian?, *Bull. Seismol. Soc. Am.* **64,** 1363–1367.

Hainzl, S., F. Scherbaum, and C. Beauval (2006). Estimating background activity based on interevent-time distribution, *Bull. Seismol. Soc. Am.* **96,** no. 1, 313–320.

Hough, S. E., J. G. Armbruster, L. Seeber, and J. F. Hough (2000). On the modified Mercalli intensities and magnitudes of the 1811–1812 New Madrid earthquakes, *J. Geophys. Res.* **105,** no. B10, 23,839–23,864.

Johnston, A. C. (1996a). Seismic moment assessment of earthquakes in stable continental regions: II. New Madrid 1811–1812, Charleston 1886 and Lisbon 1755, *Geophys. J. Int.* **126,** no. 2, 314–344.

Johnston, A. C. (1996b). Seismic moment assessment of stable continental earthquakes, III: 1811–1812 New Madrid, 1886 Charleston and 1755 Lisbon, *Geophys. J. Int.* **126,** 314–344.

Petersen, M. D., A. D. Frankel, S. C. Harmsen, C. S. Mueller, K. M. Haller, R. L. Wheeler, R. L. Wesson, Y. Zeng, O. S. Boyd, D. M. Perkins, N. Luco, E. H. Field, C. J. Wills, and K. S. Rukstales (2008). Documentation for the 2008 update of the United States National Seismic Hazard Maps, *U.S. Geol. Surv. Open-File Rept. 08-1128*, 61 pp.

Power, M., B. Chiou, N. Abrahamson, Y. Bozorgnia, T. Shantz, and C. Roblee (2008). An overview of the NGA project, *Earthq. Spectra* **24,** no. 1, 3–21.

Reasenberg, P. (1985). Second-order moment of central California seismicity, 1969–1982, *J. Geophys. Res.* **90,** 5479–5495.

Shcherbakov, R., D. L. Turcotte, and J. B. Rundle (2004). A generalized Omori's law for earthquake aftershock decay, *Geophys. Res. Lett.* **31,** L11613, doi 10.1029/2004GL019808.

Toro, G. R., and W. J. Silva (2001). Scenario earthquakes for Saint Louis, MO, and Memphis, TN, and seismic hazard maps for the central United States region including the effect of site conditions: Technical report to U.S. Geological Survey, Reston, Virginia, under Contract 1434-HQ-97-GR-02981, available at http://www.riskeng.com/downloads/scen_ceus_rept (last accessed June 2007).

Toro, G., N. Abrahamson, and J. Schneider (1997). Model of strong ground motions from earthquakes in the central and eastern North America: Best estimates and uncertainties, *Seismol. Res. Lett.* **68,** 41–57.

Tuttle, M. P., E. S. Schweig, J. D. Sims, R. H. Lafferty, L. W. Wolf, and M. L. Haynes (2002). The earthquake potential of the New Madrid Seismic Zone, *Bull. Seismol. Soc. Am.* **92,** no. 6, 2080–2089.

Tuttle, M. P., E. S. Schweig, J. Cambell, P. J. Thomas, J. D. Sims, and R. H. Lafferty (2005). Evidence for New Madrid earthquakes in A.D. 300 and 2350 B.C., *Seismol. Res. Lett.* **76,** no. 4, 489–501.

Venn, J. (1880). On the diagrammatic and mechanical representation of propositions and reasonings, *The Lond., Edin., and Dubl. Phil. Mag. and J. of Sci.* **9,** 1–18.

Wiemer, S. (2000). Introducing probabilistic aftershock hazard mapping , *Geophys. Res. Lett.* **27,** no. 20, 3405–3408.

Wiemer, S., and K. Katsumata (1999). Spatial variability of seismicity parameters in aftershock zones, *J. Geophys. Res.* **104,** 13,135–13,151.

Yeo, G. L., and C. A. Cornell (2009). A probabilistic framework for quantification of aftershock ground-motion hazard in California: Methodology and parametric study, *Earthq. Eng. Struct. Dynam.* **38,** no. 1, 45–60.

Zhuang, J., Y. Ogata, and D. Vere-Jones (2002). Stochastic declustering of space-time earthquake occurrences, *J. Am. Stat. Assoc.* **97,** no. 458, 369–380.

U.S. Geological Survey
3876 Central Ave., Suite 2
Memphis, Tennessee 38152

Manuscript received 6 January 2011